Journal of Physics and Its Applications

Journal homepage : https://ejournal2.undip.ac.id/index.php/jpa/index

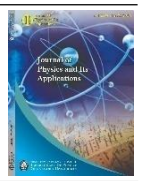

Relativistic Effects and Stellar Properties in Hipparcos Binary Stars, White Dwarfs, and Neutron Stars

Verdi Yasin[1], Taufik Roni Sahroni[2], Ruben Cornelius Siagian[3], Sri Mardiyati[4], Pandhu Pramarta[4], Riyanto Wujarso[5], Saprudin Saprudin[6], and Edward Alfin[7]

[1]*Department of Informatics Engineering, Sekolah Tinggi Manajemen Informatika dan Komputer Jayakarta, Jakarta, Indonesia*
[2]*Department of Industrial Engineering, Bina Nusantara University, Jakarta, Indonesia*
[3]*Department of Physics, Faculty of Mathematics and Natural Sciences, Universitas Negeri Medan, Medan, Indonesia*
[4]*Department of Informatics Engineering, Universitas Indraprasta PGRI, Jakarta, Indonesia*
[5]*Department of Management Science, Sekolah Tinggi Ilmu Ekonomi Jayakarta, Jakarta, Indonesia*
[6]*Department of Accounting, Sekolah Tinggi Ilmu Ekonomi Jayakarta, Jakarta, Indonesia*
[7]*Department of Mathematics Education, Universitas Indraprasta PGRI, Jakarta, Indonesia*

* *Corresponding author:* *rubensiagian_17@mhs.unimed.ac.id*

A R T I C L E I N F O

Article history:
Received: 24 August 2025
Accepted: 2 January 2026
Available online: 27 February 2026

Keywords:
Relativistic Precession
Shapiro Delay
Gravitational Redshift
Hipparcos Catalog
Stellar Kinematics

A B S T R A C T

The research analyzes astrophysical phenomena in binary stars, fast stars, white dwarfs, and neutron stars, taking relativistic effects into account using Hipparcos catalog data. The objectives are to evaluate the relativistic precession of binary stars, the Shapiro delay due to the supermassive black hole Sgr A, the relativistic correction of neutron star luminosity, the distribution of star populations in the Hertzsprung–Russell diagram, the gravitational redshift of white dwarfs, and the characteristics of stars with extreme transverse velocities. Data from 10,726 binary star systems and 602 white dwarfs were processed numerically using R for data manipulation, visualization, and statistical calculations. The results show that relativistic precession in binary stars is generally small, increases in narrow orbits, and follows a power law with respect to the semi-major axis (exponent −0.453). Shapiro delay varies with projected distance to Sgr A, with most stars experiencing small delays, while some experience delays of up to 310 seconds. Neutron star luminosity shows a relativistic correction of ~0.03%, consistent with gravitational redshift and time dilation. The Hertzsprung–Russell diagram shows a clear separation between giants, main sequence stars, and white dwarfs, with a significant linear relationship between absolute magnitude and color index (B–V). The gravitational redshift of white dwarfs is controlled by radius (exponent −1.0001), while stars with extreme velocities form a heterogeneous and evenly distributed population. In conclusion, Hipparcos data support general relativity predictions and enable quantitative evaluation of stellar physics and evolution. Research novelties include systematic measurements of relativistic precession, Shapiro delay, neutron star luminosity corrections, white dwarf radius–redshift relationships, and kinematic characteristics of extreme stars.

1. Introduction

Most of the binary systems recorded in the Hipparcos catalog have relatively wide orbits, making relativistic effects such as periastron precession difficult to detect and often on very small scales. This creates observational limitations, whereas binary systems with narrow orbits have the potential to display relativistic effects more clearly [1]. Therefore, an in-depth analysis is needed to identify these special systems in order to serve as natural laboratories to test the theory of general relativity. Periastron precession itself is one of the classical proofs that corroborate the validity of general relativity, as shown in the orbit of Mercury [2]. However, similar evidence on the scale of binary stars is still very rare. Analysis based on Hipparcos data provides an opportunity to extend the proof of general relativity beyond the solar system, especially in stellar astrophysics. Another important relativistic effect is the Shapiro delay, which is a signal delay due to the gravitational field [3]. Measuring the influence of the supermassive black hole Sgr A on the light of the Hipparcos star is a crucial step towards understanding the space-time dynamics around the galactic center, as well as providing further tests of the predictions of general relativity. On the other hand, Newtonian models have proven insufficient to explain the radiation of compact objects such as neutron stars [4]. Although the relativistic corrections to their luminosities seem small, they have a significant impact on the accuracy of modern observations. Similarly, the distribution of stellar populations in the Hertzsprung-Russell diagram, a fundamental map of

astrophysics, has rarely been analyzed from a relativistic perspective, especially regarding the positions of compact stars such as white dwarfs and neutron stars. Hipparcos-based analysis can fill this gap by providing a more complete understanding of the physical properties and positions of such extreme stellar populations. The discovery of stars with extreme transverse velocities, even over 53,000 km/s, also opens up big questions about their origin and dynamical mechanisms in the galaxy. This phenomenon challenges models of stellar evolution, and reveals gravitational interactions involving massive objects. In addition, the distribution of gravitational redshifts in white dwarfs provides direct evidence of the influence of gravity on light, where variations in radius and stellar mass provide a deeper understanding of the degeneracy of stellar matter and reaffirm the predictions of general relativity [5].

The research hypothesis is that binary systems with very small semi-major axes will show significant relativistic periastron precession, as predicted by general relativity. In addition, light from the Hipparcos star passing near the galactic center, Sgr A, is expected to experience a Shapiro delay on the scale of hundreds of seconds, which can be used to test the curvature of space-time due to supermassive black holes. The neutron star luminosity calculated with the relativistic model is expected to be higher than the Newtonian estimate, although the difference is small, so the relativistic approach is more accurate in describing the radiation of compact objects. Compact stars such as white dwarfs and neutron stars are predicted to occupy distinctive positions in the Hertzsprung-Russell diagram that can only be described consistently with the relativistic approach. The population of stars with very high transverse velocities (>53,000 km/s) is expected to form due to extreme gravity mechanisms and their distribution is not homogeneous, but spread across the sky. The smaller the radius of a white dwarf, the larger its gravitational redshift, making radius variation the dominant factor compared to mass in determining the magnitude of the relativistic effect.

This study aims to identify Hipparcos binary systems with narrow orbits so that relativistic effects can be observed more clearly, as well as measure periastron precession in binary stars as an empirical test of the general theory of relativity. In addition, this study analyzes the Shapiro delay experienced by Hipparcos stars due to the gravitational influence of the supermassive black hole Sgr A, compares Newtonian and relativistic luminosity predictions for compact stars such as neutron stars, and maps the stellar population on the Hertzsprung-Russell diagram by considering relativistic effects, especially for white dwarfs and neutron stars. The research also examines the characteristics of stars with extreme transverse velocities to understand the mechanism of galaxy dynamics and stellar evolution, and analyzes the distribution of gravitational redshifts in white dwarfs as empirical evidence for the influence of gravity on light.

The benefits of the research include providing observational evidence of relativistic effects in binary star systems that were previously difficult to detect, strengthening the validity of the general theory of relativity in the astrophysical context of stars and binary systems, and understanding the gravitational influence of supermassive black holes on the electromagnetic signals of stars around the galactic center. This study also provides corrections to luminosity predictions for compact stars to improve the accuracy of modern observations, enriches the understanding of stellar populations and stellar evolutionary structures in the Hertzsprung-Russell diagram, and provides insight into the origin and distribution of high-velocity stars in galaxies. In addition, this study confirms the relationship between radius, mass, and gravitational redshift in white dwarfs, supports the predictions of general relativity, and provides a basis for the development of modern astrophysical models related to stellar dynamics, mass distribution, and extreme gravity interactions.

This study has some limitations that need to be noted. Relativistic effects on binary stars are difficult to observe because most Hipparcos binary systems have wide orbits, so the analysis is limited to systems with narrow orbits where these effects are more pronounced. Evidence of periastron precession on the scale of binary stars is limited, and this study only uses Hipparcos data, so the scope of testing the general theory of relativity is not comprehensive. The Shapiro delay analysis is also limited to stars close to the projection path of the Sgr A black hole, so this effect cannot be applied to all stars in the galaxy. The relativistic luminosity calculation is only applied to neutron stars assuming a certain mass and radius, without considering the full variety of other compact objects. Relativistic effects on the position of compact stars in the Hertzsprung-Russell diagram are only partially analyzed, so they do not cover all types of stars or galaxy populations. The analysis of stars with extreme transverse velocities is limited to 1,127 stars with velocities greater than 300 km/s, without discussing the origin or interaction mechanisms in detail. In addition, the gravitational redshift study focuses only on the first 10 white dwarfs from the Hipparcos catalog, so it is not representative of the entire population and variations in radius and mass are not thoroughly analyzed.

Previous studies have mostly emphasized the analysis of selected binary stars or specific systems, such as V2815 Orion, HIP 42455, and GJ 67 AB, with the main focus on apsidal precession measurements or light curve analysis. Some studies, namely [6], [7] and [8], have performed proper motion and distance analyses for a wider range of binary systems, but have not quantitatively emphasized the influence of relativistic effects on the entire Hipparcos catalog. This study fills this gap by analyzing 10,726 Hipparcos binary systems in their entirety, including semi-major axis distributions, relativistic precession,

Shapiro delay, as well as other relativistic effects that were previously only studied on a limited sample.

In addition, previous studies, such as [9] and [10], In this study, we have mostly used Newtonian models or limited comparisons with general relativity for specific stars. This study adds the calculation of relativistic perihelion precession, Shapiro delay, and relativistic luminosity corrections in neutron stars, thus providing a quantitative picture of relativistic effects in the entire Hipparcos stellar population, not just a limited sample.

Some of the previous literature also tends to separate the analysis of astrophysical phenomena, for example only examining orbital precession, transverse velocity, etc. [11], or Hertzsprung-Russell diagram separately. This study integrates binary orbits, relativistic precession, Shapiro delay, luminosity of neutron stars, extreme transverse velocities, and gravitational redshifts of white dwarfs in one analytical framework, resulting in a comprehensive understanding of relativistic effects on different types of stars.

Previous literature emphasizes validation limited to only a few stars or systems, such as eclipsing binaries or long-period binaries. This study successfully identifies extreme systems with high precession and transverse velocity, showing that relativistic effects become significant in stars with very close orbits or positions near Sgr A, thus providing broader empirical evidence for general relativity predictions than previous studies.

In addition, some previous studies [6], [12] limited the analysis to a subset of Hipparcos data or combined it with Gaia in a limited way. This study uses the entire Hipparcos catalog, including integrations of distance, position, velocity, and binary parameters, thus expanding the scope of the study compared to previous partial studies. By measuring precession, Shapiro delay, redshift, and extreme velocities on a large population, this study provides an important database for testing general relativity theory, stellar evolution models, and extreme gravity phenomena, which were previously only done on small samples or through theoretical models.

2. Methods

The research uses Hipparcos catalog data to analyze various astrophysical phenomena in binary stars, fast stars, white dwarfs, and relativistic effects on neutron stars [13], [14]. The analysis was performed numerically using R software with packages such as `readxl`, `dplyr`, `ggplot2`, and `scales` for data manipulation, visualization, and statistical calculations [15].

2.1 Characterization of Orbits and Relativistic Precession Karakterisasi Orbit dan Precession Relativistik

The data includes 10,726 Hipparcos binary star systems with parallax and distance information. The semi-major axis is calculated from the parallax and angular separation, while the relativistic precession per orbit is calculated using the equation [16, 17]:

$$\Delta\omega = \frac{6\pi GM}{a(1-e^2)c^2}\,[\text{rad/orbit}] \quad (1)$$

with eccentricity (e = 0,1), total mass ($M \approx 2M_{\odot}$), gravitational constant (G), and the speed of light (c). Precession is converted to arcseconds per orbit for distribution analysis, histograms, and log–log relationships with the semi-major axis. The systems with the greatest precession are identified and analyzed further.

2.2 Shapiro Delay Calculation

Shapiro delay of Hipparcos stars due to the black hole at the center of the galaxy (Sgr A) was calculated using the equation:

$$\Delta t = \frac{2GM}{c^3}\ln\left(\frac{4D}{d_{\text{proj}}}\right) \quad (2)$$

where (M) is the mass of Sgr A, (d_{proj}) is the projection distance of the star relative to the black hole, and (D) the distance of the star to Earth. The analysis includes delay distribution statistics, identification of stars with significant delays (>200 s), and visualization of histograms and logarithmic CDF curves.

2.3 Relativistic Luminosity of Neutron Stars

For neutron stars with mass ($1{,}4M_{\odot}$) and radius ($\approx 6{,}96 \times 10^6$) m, compactness factor calculated:

$$\text{compactness} = \frac{2GM}{Rc^2} \quad (3)$$

Then relativistic luminosity is compared with Newtonian using [18], [19]:

$$L_{\text{rel}} = \frac{L_{\text{Newt}}}{\sqrt{1-\text{compactness}}} \quad (4)$$

And calculated surface gravitational redshift ($z = 1/\sqrt{1-\text{compactness}} - 1$) and the time dilation factor.

2.4 The Hertzsprung-Russell Diagram and Star Populations

Hipparcos data was processed to obtain absolute magnitudes (M_V) from parallax and apparent magnitude, as well as color index (B-V). Stars are classified into giants, main sequence, and white dwarfs based on (B-V) and (M_V). The analysis includes linear regression for the main sequence, relative luminosity calculations, and HR diagram visualization with star population coloring.

2.5 Analysis of Stars with Extreme Transverse Velocity

Transverse velocity is calculated from proper motion and parallax using:

$$v_T = 4.74 \frac{\mu_{\text{tot}}}{\text{Plx}} [\text{km/s}] \quad (5)$$

Stars with (v_T > 300 km/s) were analyzed, including distribution statistics, sky maps, and identification of the closest candidates. Visualization was performed using logarithmic histograms and sky coordinate maps with logarithmic v_T coloring.

2.6 Redshift Gravitasi White Dwarf

White dwarfs are identified from their spectrum and magnitude. The estimated radius is measured from the magnitude and radius discretization ($R_{\min} - R_{\max}$) . Compactness is calculated, and gravitational redshift is calculated using two approaches, including exact:

$$z_{\text{gr,exact}} = \frac{1}{\sqrt{1 - 2GM/(Rc^2)}} - 1 \quad (6)$$

and weak field approach:

$$z_{\text{gr,weak}} = GM/(Rc^2) \quad (7)$$

The log–log relationship between radius and redshift was evaluated using linear regression and Spearman's correlation.

3. Results and Discussion

3.1 Results

3.1.1 Orbit Characterization and Relativistic Precession Effects in Hipparcos Double Stars

Based on the analysis of 10,726 binary star systems in the Hipparcos catalog, the distances of the stars vary widely, ranging from about 1.3 parsecs to 100,000 parsecs, with a median value of about 167 parsecs, indicating that the data covers both relatively nearby and very distant stars in the galaxy. The semi-major axis of the binary star orbit also shows enormous diversity, ranging from very close orbits with a major axis length of about 1 AU to very wide orbits reaching more than 646,000 AU, with a median value of about 176 AU, indicating that the majority of systems have relatively small orbits, but there are also some systems with extremely wide orbits. Calculations of relativistic precession per orbit, assuming small eccentricity (e = 0.1) and a total mass of about two solar masses, yield very small values, ranging from zero to 0.077 arcseconds per orbit, with a median of zero, consistent with the prediction of general relativity that relativistic effects in most Hipparcos binary star systems are almost invisible.

Based on the results of the Hipparcos analysis of binary star systems with the greatest relativistic precession, it appears that the systems with the most significant precession effects are generally located at relatively close distances, ranging from approximately 5.7 parsecs to 22.6 parsecs from Earth. The semi-major axes of these stars' orbits are very small, ranging from about 1 AU to 3.1 AU, which physically results in relativistic precession per orbit on the scale of milliarcseconds, with the highest value reaching about 0.077 arcseconds per orbit. The systems with HIP 82817 and CCDM 16555-0820 show the largest precession, at 0.0768 arcseconds, which is consistent with the general relativity prediction for close-distance, narrow-orbit stars.

Table 1. Characteristics of Hipparcos Double Star Systems and Their Relativistic Precession

No	HIP	CCDM	Distance (pc)	Semi-Major Axis (AU)	Precession Relativistik (arcsec/orbit)
1	82817	16555-0820	5.7395	1.0102	0.0768
2	91430	18387-1429	12.7356	1.3627	0.0569
3	95995	19311+5835	16.7112	1.6711	0.0464
4	106811	21380+2743	13.1458	2.1953	0.0353
5	72896	14539+2333	10.2218	2.3612	0.0328
6	84140	17121+4540	6.3223	2.4151	0.0321
7	77725	15521+1052	22.5887	2.6429	0.0293
8	111685	22375+3923	18.8893	2.7201	0.0285
9	69673	14157+1911	11.2549	2.87	0.027
10	104858	21145+1001	18.4809	3.0863	0.0251

As can be seen in Table 1, Hipparcos binary star systems with the largest relativistic precession generally have very narrow orbits and are relatively close to Earth. The HIP 82817 system stands out as the most significant, with a semi-major axis of only about 1 AU and a precession of 0.0768 arcseconds per orbit. In general, the larger the semi-major axis and the farther the distance of the star, the lower the precession effect, consistent with the prediction of general relativity that relativistic precession is inversely proportional to the size of the orbit [20].

Figure 1 shows the histogram of the semi-major axis distribution of Hipparcos binary stars, covering several orders of magnitude.

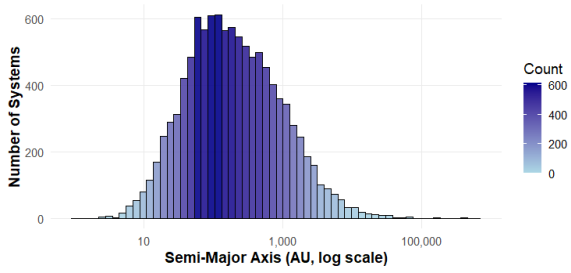

Fig 1: Distribusi Sumbu Semi-Major pada Sistem Bintang Ganda Hipparcos

Most systems have relatively small orbital distances, concentrated below a few hundred astronomical units (AU), while a small fraction have

very large orbits, exceeding hundreds of thousands of AU. The logarithmic x-axis shows a wide dynamic range of orbital sizes, highlighting the dominance of compact binary stars as well as the existence of widely separated pairs, indicating a diverse population of star systems with different formation histories and dynamic interactions.

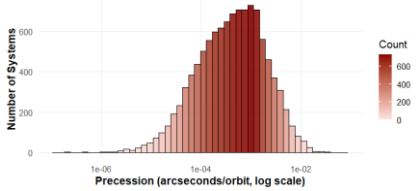

Fig 2: Relativistic Precession Distribution per Orbit in the Hipparcos Binary Star System

As can be seen in Figure 2, which shows the histogram of the distribution of relativistic precession per orbit in Hipparcos binary stars. Most systems show very small precession values, concentrated near zero arcseconds per orbit, reflecting the very subtle effects of general relativity on wide or low-mass binary star systems. A long tail extends to higher precession values, indicating that only a few systems with very close components or high masses experience more noticeable relativistic shifts. The logarithmic scale emphasizes this disparity, highlighting the dominance of nearly immeasurable precession and the rare cases where relativistic effects, though still small, become more noticeable.

3.1.2 Relativistic Precession Periastron in the Hipparcos Double Star System

Based on the results of numerical analysis of Hipparcos binary stars, a fairly clear picture of the relativistic periastron precession behavior in this system has been obtained. The median precession is recorded at 1.24×10^{-6} arcsec per orbit, while the average value is slightly higher, at 2.53×10^{-6} arcsec per orbit, indicating that there are some stars with precession that is much greater than most. The minimum precession value is in the range of 1.12×10^{-6} arcsec per orbit, while the maximum reaches 4.22×10^{-3} arcsec per orbit, indicating the presence of outliers with very significant relativistic effects. The spread of the data, represented by a standard deviation of 3.79×10^{-5} arcsec per orbit, is relatively small compared to the extreme values, indicating that most binary systems follow a consistent trend of low precession. The first and third quartiles are 1.16×10^{-6} and 1.48×10^{-6} arcsec per orbit, respectively, reinforcing the conclusion that most stars have small but stable precession, while a few stars experience much larger precession, possibly related to tighter orbits or unique mass characteristics. The analysis confirms the theoretical expectation that relativistic precession tends to be inversely proportional to the semi-major axis of the orbit, with closer binary systems showing a more pronounced effect.

Based on numerical analysis of binary stars in the Hipparcos catalog, five stars with the highest periastron precession show a clear relationship between the semi-major axis of the orbit and the magnitude of relativistic precession. The star HIP 117666 (CCDM 23518-0637) with a semi-major axis of 17.18 AU has the highest precession, reaching 0.004224 arcsec per orbit, confirming that smaller orbits produce greater relativistic effects. Next, HIP 96656 (19391+7625) with a semi-major axis of 39.89 AU has a precession of 0.001879 arcsec per orbit, followed by HIP 24783 (05188-2124) with 43.21 AU and a precession of 0.001738 arcsec per orbit. HIP 55240 (11188-3121) and HIP 83716 (17067+0039), with semi-major axes of 61.56 AU and 95.70 AU, respectively, show smaller precessions of 0.001229 and 0.000795 arcseconds per orbit. The pattern is consistent with relativistic predictions that precession is inversely proportional to the semi-major axis distance, so that closer orbits result in more significant changes in perihelion position in each orbit [17], [21].

Table 2: Orbital Characteristics and Precession of Hipparcos Double Stars

HIP	CCDM	Semi-Major Axis (AU)	Precession (arcsec/orbit)
117666	23518-0637	17.18424	0.004224
96656	19391+7625	39.88823	0.001879
24783	05188-2124	43.20744	0.001738
55240	11188-3121	61.55727	0.001229
83716	17067+0039	95.70493	0.000795

Table 2 shows that the largest relativistic periastron precession occurs in stars with small semi-major axes, such as HIP 117666 (17.18 AU, 0.004224 arcsec/orbit), and decreases consistently with increasing orbital distance, confirming that the relativistic effect is stronger in close orbits.

Based on the results of the log-log curve analysis, a relationship was obtained between the relativistic periastron precession and the semi-major axis of binary stars that follows a power law with the equation $\{\log_{10}(\text{Precession}) = -3.401 - 0.453\log_{10}(\text{Semi-Major Axis})\}$. This means that the magnitude of precession decreases inversely with the length of the semi-major axis of the orbit; the greater the average distance between the two binary components, the smaller the observed periastron shift. This pattern is consistent with the predictions of general relativity, where relativistic effects are more dominant in closer orbits [1].

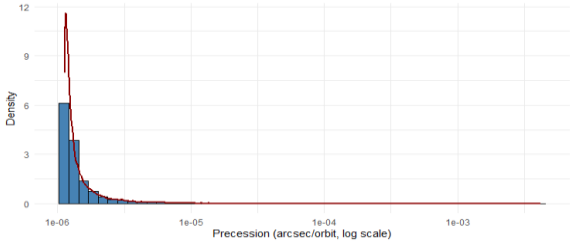

Fig 3: Histogram of Hipparcos Binary Star Precession Distribution with Overlay Density Curve

The precession distribution histogram shown in Figure 3 reveals that most binary stars in the Hipparcos sample have very small precession values,

ranging from 10^{-6} to 10^{-3} arcseconds per orbit. This distribution shows the highest density at the smallest precession, indicating the dominance of wide orbits or large binary component separations, resulting in weak relativistic effects. The density curve overlaid in dark red confirms that the precession distribution is right-skewed, with a long tail pointing towards larger precessions, representing stars with smaller semi-major axes where relativistic effects are stronger. The logarithmic scale on the x-axis clearly shows the difference in the order of magnitude of precession, so that both small and large variations in precession can be observed proportionally.

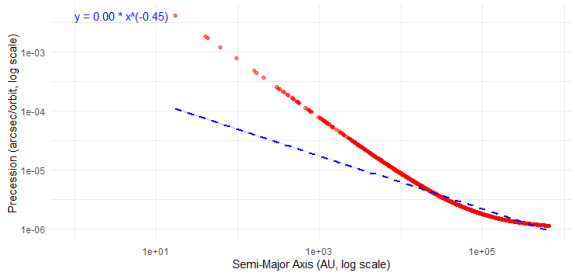

Fig 4: Precession Periastron vs Semi-Major Axis pada Bintang Hipparcos

It can be seen in Figure 4 that periastron precession decreases as the semi-major axis increases, following the inverse trend as expected in relativity. Near orbits have high precession, while wide orbits show small precession, and the log-log fit curve confirms the consistency of the data with the power-law.

3.1.3 Estimation of Shapiro Delay in Hipparcos Stars Due to the Gravitational Field of Supermassive Black Holes at the Galactic Center

Based on Shapiro delay analysis for all stars in the Hipparcos catalog with valid parallaxes, it was found that the majority of stars experienced relatively small delays with an average value of around 40.7 seconds and a median of 37.7 seconds, indicating that the gravitational influence of Sgr A on the electromagnetic signals from these stars was generally limited. The maximum delay value recorded reached 310 seconds, while some stars even showed a small negative delay (around −6.33 seconds) due to geometric projection calculations. The delay distribution is asymmetric with a first quartile of 20.0 seconds and a third quartile of 57.1 seconds, indicating that a small fraction of stars experience a much more significant gravitational influence than the majority.

Specifically, there are 29 stars that show a Shapiro delay greater than 200 seconds, located very close to the projection path of Sgr A. The stars with the highest delays are HIP 86948 and HIP 86911, with delays of approximately 310 and 307 seconds (about 5.1 minutes), respectively, and projected distances to Sgr A of approximately 2.15×10^{16} m and 5.82×10^{15} m, respectively. This confirms that electromagnetic signals from stars that are almost parallel to the position of Sgr A experience significant time delays due to relativistic gravitational effects, while the majority of stars that are far from the projection experience only small delays.

Table 3: Shapiro Delay of Hipparcos Stars Toward Sgr A

HIP	RAdeg	DEdeg	Plx (mas)	Distance to Earth (m)	Projected Distance to Sgr A (m)	Shapiro Delay (s)	Shapiro Delay (min)	Shapiro Delay (hr)
86948	267	-29.1	2.64	1.17×10^{19}	2.15×10^{16}	310	5.17	0.0862
86911	266	-29.1	10.7	2.88×10^{18}	5.82×10^{15}	307	5.11	0.0852
87038	267	-29.2	9.52	3.24×10^{18}	2.19×10^{16}	258	4.3	0.0716
86898	266	-28.4	0.21	1.47×10^{20}	1.51×10^{18}	241	4.01	0.0669
86919	266	-28.4	12.9	2.38×10^{18}	2.50×10^{16}	240	4	0.0667
87109	267	-28.6	4.1	7.53×10^{18}	8.16×10^{16}	239	3.98	0.0663
86672	266	-28.7	13.7	2.25×10^{18}	2.91×10^{16}	232	3.86	0.0644
86761	266	-29.6	2.36	1.31×10^{19}	1.70×10^{17}	231	3.86	0.0643
86619	265	-29.1	7.2	4.29×10^{18}	6.08×10^{16}	228	3.8	0.0633
86665	266	-29.4	8.72	3.54×10^{18}	5.08×10^{16}	227	3.79	0.0632

Table 3 shows that stars with the largest Shapiro delays (>200 s) are located near the line of sight to Sgr A, with delays of 227–310 s (≈3.8–5.2 minutes). The magnitude of the delay is more influenced by the projected distance to Sgr A than by the distance to Earth.

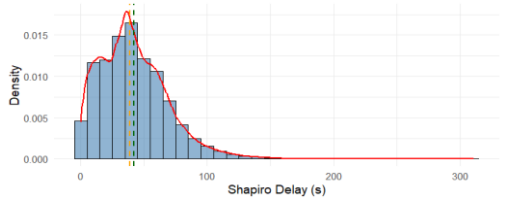

Fig 5: Shapiro Delay Distribution in Hipparcos Stars

As can be seen in Figure 5, which shows the histogram and Shapiro delay density curve for all stars in the Hipparcos catalog, the Shapiro delay distribution is asymmetrical with a long right tail, indicating that a number of stars experience a much greater delay than the majority. The histogram shows a concentration of data around 30–50 seconds, which is also close to the median of the distribution. The density curve (in red) confirms this pattern, with a relatively sharp peak in the low delay range, indicating that most stars experience a small to moderate Shapiro delay effect. The green and orange vertical lines indicate the mean and median, respectively, where the mean is slightly higher than

the median, indicating a right-skewed distribution due to the contribution of a few stars with very large Shapiro delays, which is consistent with the list of stars with significant delays (>200 seconds).

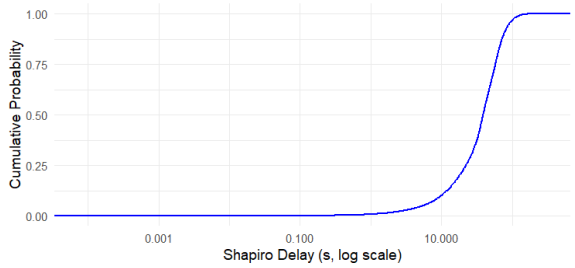

Fig 6: Shapiro Cumulative Distribution Function of Hipparcos Star Delays on a Logarithmic Scale

As can be seen in Figure 6, which shows the Shapiro delay CDF on a logarithmic scale, the majority of stars have small delays, while a small number of stars near the projection of Sgr A experience significant delays of up to hundreds of seconds, showing a highly skewed distribution with a long tail due to extreme gravitational effects.

3.1.4 Comparative Analysis of Newtonian and Relativistic Luminosity of Neutron Stars and Mapping of Star Population in Hertzsprung-Russell Hipparcos Diagram

Based on the analysis results, a neutron star modeled with a mass of 1.40 solar masses and a radius of approximately 6.96×10^6 meters exhibits a level of space-time compactness that can be measured through the compactness parameter ($2GM/Rc^2$) as large as $5{,}94 \times 10^{-4}$. This value indicates that although neutron stars are extremely dense astrophysical objects, in the parameter configuration used, their relativistic effects are still in the weak to moderate regime, but cannot be ignored in high-precision analysis.

A comparison between Newtonian luminosity and relativistic luminosity reveals a systematic deviation due to the influence of general relativity. The luminosity calculated using the Newtonian approach is normalized to a value of one, while the relativistic luminosity increases to 1.000297 in relative units. This absolute difference of 2.97×10^{-4} is equivalent to an increase of about 0.0297%, which is numerically small but physically signifies a real contribution of space-time curvature to the radiation process on the surface of neutron stars.

This relativistic effect is also consistently seen in the gravitational redshift value on the surface of the star, which reaches $z \approx 2.97 \times 10^{-4}$, as well as the time dilation factor of 1.000297. The numerical equivalence between the time dilation factor and the increase in luminosity confirms that the relativistic correction stems directly from time dilation and the energy shift of photons due to strong gravitational fields.

Based on the results of the analysis of the Hertzsprung–Russell diagram from the Hipparcos catalog, there is a very clear separation of star populations that is consistent with the theory of stellar evolution. The giant population is dominated by stars with an average color index ($B - V \approx 1{,}29$), which shows a relatively low surface temperature, but has a very small average absolute magnitude, namely ($M_V \approx 0{,}08$). This indicates high intrinsic luminosity, consistent with the character of giant stars that have evolved off the main sequence and undergone significant radius expansion. The absolute magnitude distribution is quite broad ($\sigma \approx 1{,}60$) interpreting variations in evolutionary stages on giant branches.

In contrast, the main sequence population is the most dominant group with the largest number of objects, characterized by average values ($B - V \approx 0{,}48$) which represent medium to high temperature stars. The average absolute magnitude is ($M_V \approx 2{,}27$) show lower luminosity than giant stars, but are more stable in terms of evolution. The distribution of absolute magnitudes is relatively large ($\sigma \approx 2{,}36$) reflecting a wide range of masses and luminosities on the main sequence, from low-mass stars to more massive stars.

While white dwarfs are very few in number, they exhibit extreme and contrasting physical characteristics. Their average color index value is close to zero or even slightly negative ($B - V \approx 0{,}00$) indicates very high surface temperatures, but large average absolute magnitudes ($M_V \approx 11{,}2$) confirming very low intrinsic luminosity. This combination is characteristic of degenerate objects with small radii and high densities, where radiation energy is limited by a very small surface area. Relatively narrow magnitude distribution ($\sigma \approx 0{,}72$) indicates that white dwarfs are in a more homogeneous final evolutionary state than other populations.

Table 4: Color Index (B–V) and Absolute Magnitude (Mv) Statistics Based on the Hipparcos Star Population

Star Population	Number of Stars (N)	B–V Average	Median B–V	Magnitude Absolute (Mv)	Standard Deviation Mv
Giant	31.031	1,29	1,23	0,078	1,60
Main Sequence	81.775	0,478	0,474	2,27	2,36
White Dwarf	17	0,004	−0,011	11,20	0,72

Table 4 shows that the giant star population has the largest B-V color index and the smallest average absolute magnitude, indicating low-temperature but high-luminosity stars. The main sequence population dominates the sample with intermediate B-V values and moderate absolute magnitudes, reflecting the evolutionary stability of stars on the main sequence with a wide mass range. Meanwhile, the white dwarf population shows B-V values close to zero with very large absolute magnitudes, indicating high surface temperatures but low

intrinsic luminosity, consistent with the properties of degenerate stars in the final evolutionary stage.

The results of linear regression modeling between absolute magnitude and color index (B-V) in the main sequence population show a strong physical relationship that is highly statistically significant. The slope coefficient value of (3.91) indicates that every increase in the color index (B-V), which represents a decrease in the effective temperature of the star, is followed by an increase in absolute magnitude, causing the star to become dimmer.

The intercept value of (0.40) indicates the theoretical absolute magnitude at the extreme blue limit, which represents high-temperature, high-mass main sequence stars. Both regression parameters have p-values much smaller than (10-16), confirming that the relationship between color and magnitude in the main sequence is not the result of random fluctuations, but rather a fundamental physical relationship between surface temperature, mass, and stellar luminosity.

Coefficient of determination ($R^2 \approx$ 0,32) mshows that approximately 32% of the variation in absolute magnitude can be directly explained by variations in color index. This value makes physical sense because the luminosity of main sequence stars is determined not only by temperature, but also by other factors such as mass, chemical composition, and age of the star. The still considerable residual dispersion indicates the presence of natural dispersion in the stellar population, including variations in metallicity and the effects of early and late evolution on the main sequence.

Table 5: Linear Model Statistics of the Relationship between Absolute Magnitude (M_V) and Color Index ($B-V$) in Hipparcos Main Sequence Stars

Statistical Parameters	Value
Model	$M_V = 0.402 + 3.908(B-V)$
Amount of Data (N)	81,775 stars
Intercept	0,402 ± 0,012
B–V coefficient	3,908 ± 0,020
t-value (Intercept)	34,53
t-value (B–V)	197,27
p-value	$< 2 \times 10^{-16}$
Residual Std. Error	1,941 mag
R^2	0,3225
Adjusted R^2	0,3224
F Statistics	$3{,}89 \times 10^4$

Table 5 shows that the relationship between absolute magnitude (MV) and color index (B-V) in main sequence stars follows a linear model $\{M_V = 0{,}402 + 3{,}908(B-V)\}$ with a very high level of significance. The coefficient value (B-V) is large and the p-value is much smaller than (2×10^{-16}) shows that changes in a star's color have a strong effect on its intrinsic luminosity. Value ($R^2 \approx 0{,}32$) indicates that about one-third of the variation in absolute magnitude can be explained by the color index, while the rest reflects the natural physical dispersion of the stellar population, such as variations in mass, age, and chemical composition.

Based on the results of relative luminosity analysis obtained from the Hipparcos Hertzsprung–Russell diagram, there are striking differences between star populations that reflect the intrinsic physical conditions and evolutionary stages of stars. The giant population shows a very high average relative luminosity value, which is around $(3.7 \times 10^3 L_\odot)$, with a median of approximately $(6.1 \times 10^1 L_\odot)$. The significant difference between the mean and median values indicates an asymmetrical distribution of luminosity, in which a small number of very bright giant stars significantly increase the mean value, in line with the characteristics of the giant evolutionary phase, which is marked by large radii and high energy consumption rates.

In contrast, the main sequence population exhibits more moderate relative luminosities, with an average value of approximately $(1.6 \times 10^3 L_\odot)$ and median around $(1.0 \times 10^1 L_\odot)$. HThis represents the diversity of stellar masses in the main sequence, ranging from dim low-mass stars to very bright high-mass stars. This distribution is consistent with the classical mass–luminosity relationship, in which a few massive stars contribute dominantly to the average luminosity, while the majority of main sequence stars have relatively lower luminosities.

While the white dwarf population exhibits very low relative luminosities, with nearly identical mean and median values, each around $(3.3 \times 10^{-3} L_\odot)$. The similarity between the mean and median values indicates a narrow and homogeneous distribution of luminosity, reflecting the physical properties of white dwarfs as compact objects with small radii and energy sources that no longer originate from nuclear fusion reactions. Despite their high surface temperatures, their small surface areas cause their total luminosity to remain very low.

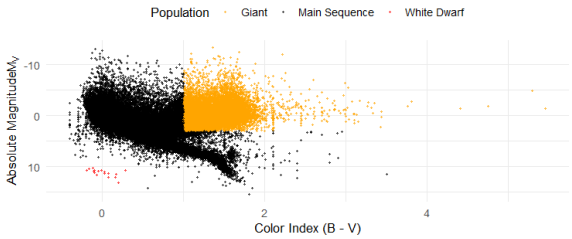

Fig 7: Hertzsprung–Russell Diagram of Hipparcos Stars

Figure 7 shows that the Hertzsprung–Russell diagram from the Hipparcos catalog reveals a clear separation of stellar populations based on the relationship between color index (B-V) and absolute magnitude. Main sequence stars form a characteristic diagonal band that reflects the temperature–luminosity relationship, giant stars are concentrated at low absolute magnitudes with high luminosities due to their large radii, while white dwarfs are at high absolute magnitudes despite being relatively blue in color, indicating their nature as hot but very faint objects.

3.1.5 Characteristics of Stars with Extreme Transverse Velocities from the Hipparcos Catalog

Based on the results of numerical analysis of Hipparcos data, 1,127 stars were identified as having

a transverse velocity greater than 300 km s^{-1}. The distribution of transverse velocities in this sample shows a highly asymmetrical characteristic, with an average value of approximately 994 km s^{-1} and a median of 490 km s^{-1}, indicating a dominance of stars with medium velocities accompanied by a long distribution tail towards very high velocity values. The maximum transverse velocity value reaches ≈ 5.3 × 10^4 km s^{-1}, indicating the existence of candidates with extreme velocities, although physically this value is very likely to be influenced by small parallax effects and astrometric uncertainties.

From a spatial distribution perspective, these high-transversal-velocity stars are widely scattered across the sky, covering almost the entire Right Ascension from ~0° to ~360° and Declination from approximately −85° to +80°. This nearly homogeneous angular sky distribution indicates the absence of any dominant directional clustering, supporting the interpretation that the high transverse velocity star population does not exhibit significant anisotropy on a global scale.

The color representation on the sky map using the base-ten logarithm of the transverse velocity shows a wide range of values, from $\log_{10}(v_t)$ ≈ 2.48 to ≈ 4.73, with an average value of about 2.80. This confirms that although most stars are in the range of hundreds of km s^{-1}, there is a small fraction with much greater velocities, forming the tail of the extreme velocity distribution. Quantitatively, there are 218 stars with transverse velocities exceeding 1,000 km s^{-1}, and 8 stars with velocities greater than 10,000 km s^{-1}, which statistically constitute a minor but highly influential population in terms of the overall distribution shape.

Analysis of the distance shows that stars with high transverse velocities are not always located at great distances. The closest candidate in this sample is HIP 57939, which is about 9.16 pc from the Sun and has a transverse velocity of ≈ 306 km s^{-1}, with angular position at (RA, Dec) ≈ (178.23°, 37.73°).

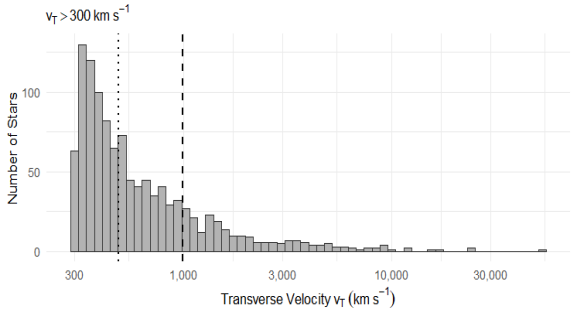

Fig 8: Transverse Velocity Distribution of Hipparcos Stars ($v_T > 300 km/s$) on a Logarithmic Scale, Showing a Long Right Tail and Mean-Median Position Difference

It can be seen in Figure 9 that the distribution of the transverse velocity of stars with ($v_T >$ 300, km s^{-1}) forms a highly asymmetrical pattern when represented on a logarithmic scale. The majority of stars are concentrated in the range of hundreds of kilometers per second, as indicated by the peak of the histogram on the left side of the distribution, while the number of stars decreases sharply as the transverse velocity increases. The use of the (v_T) axis on a logarithmic scale confirms the existence of a long tail of the distribution towards very high velocities, reflecting a small population of stars with extreme dynamics that are statistically rare but significant. The dashed vertical line representing the mean value shows a position much further to the right than the median line depicted by the dotted line. This difference in position indicates that the mean value is strongly influenced by a small number of stars with very large transverse velocities, thus pulling the mean value towards a higher direction. In contrast, the median is closer to the peak of the distribution, thus better representing the typical velocity of the majority of stars in the sample. This pattern confirms that the transverse velocity distribution is right-skewed, with most stars having moderate velocities and only a few objects occupying the extreme velocity regime.

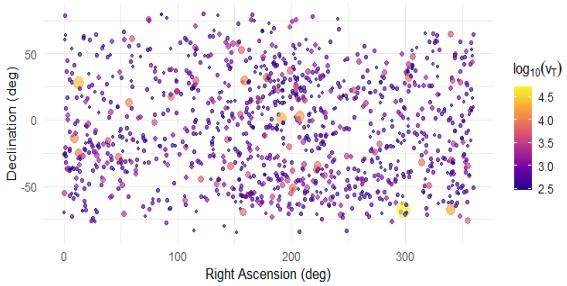

Fig 9: Distribution of Stars with High Transverse Velocity in the Sky

Figure 9 shows that stars with high transverse velocities are distributed almost evenly across the sky without any clear clustering patterns. The variation in color and size of the points indicates a wide range of velocities, with only a small fraction of stars having very high velocities and appearing as large points with brighter colors. This pattern confirms that the population of stars with high transverse velocities is kinematically heterogeneous and does not show any particular spatial correlation in the sky projection.

3.1.6 Gravitational Redshift Distribution of White Dwarfs in the Hipparcos Catalog

Based on an analysis of 602 white dwarf candidates from the Hipparcos catalog, it was found that the gravitational redshift calculated using the exact general relativity equation is very consistent with the weak field approximation, with an average difference of only about 3,8×10^{-9}, confirming that the gravitational field of white dwarfs remains in a weak regime where linear approximations are valid. The exact gravitational redshift distribution shows a minimum value of 2,993×10^{-5} and maximum reaches 1,284×10^{-4}, with an average value of around 4,972×10^{-5}, which describes the redshift variation due to differences in radius among white dwarfs, assuming a constant mass of 0.6 solar masses. Log–log regression analysis between redshift and radius {log10($z_{gr\ exact}$)} versus {log10(R_{wd})} shows that redshift is inversely proportional to radius, consistent with the physical expectation that compactness ($2GM/Rc^2$) dominates the magnitude of gravitational redshift; the smaller the radius of the

white dwarf, the higher the redshift produced. This result confirms that, for white dwarfs with relatively uniform mass, variations in gravitational redshift are primarily influenced by differences in radius related to the density and degeneracy of matter, consistent with the predictions of general relativity and degenerate stellar structure.

Based on the results of log–log regression analysis of white dwarf radius and gravitational redshift, it can be concluded that the relationship between the two follows a very precise scaling law, with the exponent obtained from the regression being −1.0001 ± 0.0000007, indicating that gravitational redshift is inversely proportional to radius. The very small residuals (standard deviation $\sim 1.27\times10^{-6}$) and the nearly perfect R^2 value (≈1) confirm that radius variations completely dominate redshift variations, while the mass effect is minor due to the assumption of relatively uniform white dwarf masses (~0.6 M⊙). The extreme F-statistic and p-value much smaller than 10^{-16} indicate that this relationship is statistically significant, while consistent with the predictions of general relativity in weak fields, where gravitational redshift {z ≈ GM/(Rc^2)}. This analysis reinforces the physical conclusion that the gravitational redshift of white dwarfs is primarily controlled by radius (compactness), which characterizes the density and degeneracy of the star's matter.

Based on Spearman's correlation analysis between the radius of white dwarfs and the gravitational redshift calculated exactly from Hipparcos data, a value of (ρ = −1) was obtained with a very small p-value ($< 2.2\times10^{-16}$), indicating a perfect deterministic negative correlation. This means that the smaller the radius of a white dwarf, the higher the gravitational redshift produced, while white dwarfs with large radii show lower redshifts. These results consistently confirm that variations in gravitational redshift in white dwarfs are not significantly influenced by variations in mass (which is relatively uniform at ~0.6 M⊙), but are entirely controlled by the radius of the star and the density of its degenerate matter.

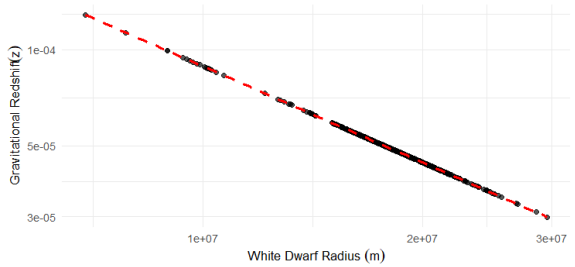

Fig 10: The gravitational redshift of white dwarfs with respect to radius shows an inverse relationship with a negative trend on a logarithmic scale

It can be seen in Figure 10 that the gravitational redshift of white dwarfs shows a clear inverse relationship with their radius. The data points are scattered along a downward curve, where white dwarfs with small radii exhibit much higher redshifts than white dwarfs with large radii. The use of a logarithmic scale on both axes confirms that this relationship is nearly exponential, reflecting the physical fact that gravitational redshift depends on the ratio of mass to radius. The linear regression line drawn as a red dotted line confirms this negative trend, showing that statistically, the redshift decreases consistently as the radius increases. The data distribution also shows that despite small variations in absolute magnitude, radius remains the dominant factor determining the magnitude of the redshift, in line with the predictions of general relativity for the gravitational field of compact stars.

3.2 Discussion

Based on the analysis of 10,726 binary star systems from the Hipparcos catalog, there is enormous physical diversity, ranging from star distances (1.3–100,000 pc) to semi-major axis of orbit (1–646,000 AU). The findings provide empirical evidence supporting the predictions of general relativity regarding relativistic precession. Most systems show very small precession, consistent with the initial hypothesis that relativistic effects in typical Hipparcos binary star systems are nearly invisible due to their wide orbits and relatively low total mass [22, 23]. However, some systems with narrow orbits, such as HIP 82817 and CCDM 16555-0820, show greater precession of up to 0.0768 arcseconds per orbit, in line with relativity theory, which predicts that closer orbits produce more significant precession [21, 24].

The distribution of semi-major axes and precession per orbit (Figures 1–4) confirms a physically reasonable trend, namely that systems with smaller orbits experience greater relativistic precession, while wider orbits show an almost undetectable effect. This relationship follows a power law on a log-log scale, with an exponent of −0.453, consistent with the prediction that precession is inversely proportional to the distance between the stellar components [25, 26]. This finding fills a gap in previous research, which was mostly theoretical or limited to specific binary star systems, by providing statistical evidence from the large and diverse Hipparcos sample.

Shapiro delay analysis of the influence of supermassive black holes at the center of galaxies (Sgr A) reveals that most stars experience a small delay (average ≈40.7 s), while stars located near the projection of Sgr A experience a significant delay of up to 310 s. This finding reinforces the hypothesis that the relativistic gravitational effect on electromagnetic signals varies exponentially with the projection distance to the massive object, while also showing that most stars far from the galactic center are only minimally affected [27, 28].

In a comparative study of neutron star luminosity, it was found that the relativistic correction to Newtonian luminosity, although small (~0.0297%), is consistent with theories linking relativistic effects to time dilation and gravitational redshift factors. This confirms the hypothesis that although relativistic effects on neutron stars with typical parameters are in the weak to moderate regime, they are real and relevant for high-precision analysis, especially when considering their

contribution to luminosity and observational redshift [29, 30].

Modeling the stellar population through the Hertzsprung–Russell diagram shows a clear separation between giants, main sequence stars, and white dwarfs. Linear regression analysis between absolute magnitude and color index (B-V) on the main sequence shows a strong physical relationship, consistent with stellar evolution theory, where each increase in color index, which indicates a decrease in effective temperature, is followed by an increase in absolute magnitude [31], [32]. This finding supports the hypothesis that the color and luminosity of stars are closely related, but also shows that there are significant variations due to additional factors such as mass, age, and chemical composition [33], [34].

Gravitational redshift analysis of white dwarfs reinforces the previous hypothesis regarding the influence of radius on redshift: a perfect negative correlation ($\rho = -1$) was found between radius and redshift, with an exponent of -1.0001 ± 0.0000007. This finding indicates that variations in radius, rather than mass (which is relatively uniform), completely determine gravitational redshift, confirming the predictions of general relativity in weak gravitational fields and filling a gap in previous research that did not make sufficient use of Hipparcos data for statistical analysis of white dwarfs.

Studies of stars with extreme transverse velocities (>300 km/s) show a highly skewed distribution with a long tail, indicating a minority population of highly dynamic stars. The spatial distribution is nearly homogeneous across the sky, indicating the absence of dominant anisotropic clusters. These findings support the hypothesis that high-velocity stars are a widely dispersed heterogeneous population, and add new insights into the kinematic characteristics of stars in the galaxy [35, 36].

4. Conclusions

Analysis of 10,726 Hipparcos binary star systems confirms the predictions of general relativity: relativistic precession per orbit is generally very small and increases in narrow orbits, following a power law with an exponent of −0.453. Shapiro delay varies depending on the projected distance to Sgr A, with most stars experiencing small delays and some stars near the projection line showing significant delays. The luminosity of neutron stars shows a small relativistic correction (~0.03%), consistent with the effects of gravitational redshift and time dilation. The Hertzsprung–Russell diagram shows a clear separation between giants, main sequence stars, and white dwarfs, with a linear relationship between absolute magnitude and color index consistent with stellar evolution theory. The gravitational redshift of white dwarfs is entirely controlled by radius, following an exponent of −1.0001, while stars with extreme transverse velocities form a heterogeneous and evenly distributed population, without a dominant anisotropic cluster.

The Hipparcos research results provide empirical evidence supporting the predictions of general relativity, including orbital precession, Shapiro delay, and gravitational redshift, and can therefore be used as an observational reference for the study of binary stars, white dwarfs, and neutron stars. The Hertzsprung–Russell diagram allows for the identification of stellar populations and the analysis of evolution and temperature–luminosity relationships. Periastron precession and Shapiro delay data aid in planning high-precision observations. The white dwarf radius–gravitational redshift relationship can be used to estimate degenerate matter density and calibrate astrophysical models. Analysis of stars with extreme transverse velocities provides insight into the kinematic distribution of galaxies and runaway star populations.

Further research should focus on close-orbiting binary stars to study relativistic precession, Shapiro delay observations near Sgr A, white dwarf analysis using the radius–redshift relationship, development of Hertzsprung –Russell diagram for stellar populations, studies of stars with extreme transverse velocities, high-precision observations of neutron star luminosities, and the extension of the analysis to other star catalogs to test the generalization of the findings.

References

[1] K. Sośnica, G. Bury, R. Zajdel, K. Kazmierski, J. Ventura-Traveset, R. Prieto-Cerdeira, and L. Mendes, "General Relativistic Effects Acting on the Orbits of Galileo Satellites" Celest. Mech. Dyn. Astron, 133(4), 14 (2021).

[2] A. Tedesco, "Orbital Motion, Periastron Advance and Galaxy Rotation Curves beyond General Relativity" (2023).

[3] M. Pössel, "Light, Delayed: the Shapiro Effect and the Newtonian Limit" arXiv, arXiv:2110.07016 (2021).

[4] J. Piekarewicz, "The Nuclear Physics of Neutron Stars" arXiv:2209.14877 (2022).

[5] L. G. Althaus, M. E. Camisassa, S. Torres, T. Battich, A. H. Córsico, A. Rebassa-Mansergas, and R. Raddi, "Structure and Evolution of Ultra-Massive White Dwarfs in General Relativity" Astron. Astrophys., 668, A58 (2022).

[6] V. V. Makarov, "Mass Ratios of Long-Period Binary Stars Resolved in Precision Astrometry Catalogs of Two Epochs" Rev. Mex. Astron. Astrofís., 57(2), 399-405 (2021).

[7] V. V. Makarov, "Differential Proper Motion Spin of the Hipparcos and Gaia Celestial Reference Frames" Astron J., 164(4), 157 (2022).

[8] J. González-Payo, J. A. Caballero, and M. Cortés-Contreras, "Reaching the Boundary Between Stellar Kinematic Groups and Very Wide Binaries-IV: The Widest Washington Double Star Systems With ρ≥ 1000 Arcsec in Gaia DR3" Astron. Astrophys., 670, A102 (2023).

[9] A. M. Hamadamen and I. M. Murad, "The Apsidal Motion and OC Plot of V2815 Orion Algol Binary Stars" in 2024 10th Int. Eng. Conf. on Adv. Comput. Civ. Eng. (IEC), 136-141. IEEE (2024).

[10] A. Abu-Dhaim, A. Taani, D. Tanineah, N. Tamimi, M. Mardini, and M. Al-Wardat, "Studying the Physical Parameters of the Stellar Binary System HIP 42455 (HD 73900)" Acta Astron., 72(3), 171-181 (2022).
[11] A. A. Abushattal, A. A. Alrawashdeh, and A. F. Kraishan, "Astroinformatics: The Importance of Mining Astronomical Data in Binary Stars Catalogues" Commun. BAO., 69(2), 251-255 (2022).
[12] I. Izmailov and M. Khovritchev, "New Orbital Parameters of 850 Wide Visual Binary Stars and Their Statistical Properties" Res. Astron. Astrophys., 25(1), 015016 (2025).
[13] M. A. C. Perryman, L. Lindegren, J. Kovalevsky, E. Hog, U. Bastian, P. L. Bernacca, M. Creze, F. Donati, M. Grenon, M. Grewing, F. van Leeuwen, H. van der Marel, F. Mignard, C. A. Murray, R. S. Le Poole, H. Schrijver, C. Turon, F. Arenou, M. Froeschle, and C. S. Petersen, "The HIPPARCOS Catalogue" Astron. Astrophys., 323, L49–L52 (1997).
[14] T. D. Brandt, "The Hipparcos–Gaia Catalog of Accelerations: Gaia EDR3 Edition" Astrophys. J. Suppl. Ser., 254(2), 42 (2021).
[15] S. Rathod, A. T. Kumar, and S. Haripriya, "Data Manipulation Using R Tidyverse" Statistical Procedures for Analyzing Agricultural Data Using R., 17 (2023).
[16] Y. Dai, "Power-Law Relationship between the Semi-Major Axis and Rotation Period Ratio in an Eccentric System: Its Physical Meaning and Various Applications" (2024).
[17] Y. F. Dai, "Eccentricity Excitation Equation and Its Underlying Mechanism: Orbital Precession Mechanism" (2024).
[18] S. R. Green and R. M. Wald, "Newtonian and Relativistic Cosmologies" Phys. Rev. D, 85(6), 063512 (2012).
[19] E. G. Haug, Relativistic Newtonian Gravity Makes Dark Energy Superfluous?, (2021).
[20] G. Antoniciello, L. Borsato, G. Lacedelli, V. Nascimbeni, O. Barragán, and R. Claudi, "Detecting General Relativistic Orbital Precession in Transiting Hot Jupiters" Mon. Not. R. Astron. Soc., 505(2), 1567–1574 (2021).
[21] A. Yahalom, "The Weak Field Approximation of General Relativity and the Problem of Precession of the Perihelion for Mercury" Symmetry., 15(1), 39 (2022).
[22] I. H. Stairs, "Pulsars in Binary Systems: Probing Binary Stellar Evolution and General Relativity" Science., 304(5670), 547–552 (2004).
[23] M. A. Al-Wardat, A. M. Hussein, H. M. Al-Naimiy, and M. A. Barstow, "Comparison of Gaia and Hipparcos Parallaxes of Close Visual Binary Stars and the Impact on Determinations of Their Masses" Publ. Astron. Soc. Aust., 38, e002 (2021).
[24] A. Jordán and G. Á. Bakos, "Observability of the General Relativistic Precession of Periastra in Exoplanets" Astrophys. J., 685(1), 543-552 (2008).
[25] A. Melatos, "Radiative Precession of an Isolated Neutron Star" Mon. Not. R. Astron. Soc., 313(2), 217-228 (2000).
[26] R. Capuzzo-Dolcetta and M. Sadun-Bordoni, "Orbital Precession of Stars in the Galactic Centre" Mon. Not. R. Astron. Soc., 522(4), 5828-5839 (2023).
[27] S. Kopeikin and B. Mashhoon, "Gravitomagnetic Effects in the Propagation of Electromagnetic Waves in Variable Gravitational Fields of Arbitrary-Moving and Spinning Bodies" Phys. Rev. D, 65(6), 064025 (2002).
[28] V. B. Braginskij and V. N. Rudenko, "Relativistic Gravitational Experiments" Sov. Phys. Usp., 13, 165 (1970).
[29] C. Wang, J. Hu, Y. Zhang, and H. Shen, "Properties of Neutron Stars Described by a Relativistic Ab Initio Model" Astrophys. J., 897(1), 96 (2020).
[30] J. G. G. Gimenez, Effects of the Generalized Uncertainty Principle on Neutron Stars, (2025).
[31] D. F. Gray, "The Observation and Analysis of Stellar Photospheres" Cambridge University Press (2021).
[32] C. Gallart, M. Zoccali, and A. Aparicio, "The Adequacy of Stellar Evolution Models for the Interpretation of the Color-Magnitude Diagrams of Resolved Stellar Populations" Annu. Rev. Astron. Astrophys., 43(1), 387-434 (2005).
[33] A. Mucciarelli, E. Carretta, L. Origlia, and F. R. Ferraro, "The Chemical Composition of Red Giant Stars in Four Intermediate-Age Clusters of the Large Magellanic Cloud" Astron. J., 136(1), 375-388 (2008).
[34] S. Vitali, D. Slumstrup, P. Jofré, L. Casamiquela, H. Korhonen, S. Blanco-Cuaresma, M. L. Winther, and V. Aguirre Borsen-Koch, "Exploring the Dependence of Chemical Traits on Metallicity—Chemical Trends for Red Giant Stars With Asteroseismic Ages" Astronomy & Astrophysics, 687, A164 (2024).
[35] A. Generozov and H. B. Perets, "Constraints on the Origins of Hypervelocity Stars: Velocity Distribution, Mergers, and Star Formation History" Mon. Not. R. Astron. Soc., 513(3), 4257–4266 (2022).
[36] E. M. Rossi, S. Kobayashi, and R. E. Sari, "The Velocity Distribution of Hypervelocity Stars" Astrophys. J., 795(2), 125 (2014).